

# Excitation of Surface Acoustic Waves and Lamb Waves at Superhigh Frequencies in a Diamond-Based Piezoelectric Layered Structure

G. M. Kvashnin<sup>a, \*</sup>, B. P. Sorokin<sup>a, \*\*</sup>, and S. I. Burkov<sup>b</sup>

<sup>a</sup>Technological Institute for Superhard and New Carbon Materials, Moscow, Troitsk, 142190 Russia

<sup>b</sup>Siberian Federal University, Krasnoyarsk, 660041 Russia

\*e-mail: genmih@yandex.ru

\*\*e-mail: bpsorokin1953@yandex.ru

Received January 22, 2020; revised March 11, 2020; accepted July 7, 2020

**Abstract**—The authors have carried out an experimental and theoretical study of the propagation of surface acoustic waves (SAW)—Rayleigh, Sezawa and SH-modes, as well as Lamb waves in Me-IDT/AlN/(100) diamond (Me = Pt, Al) piezoelectric layered structures with a SAW resonator configuration. The types of modes are identified and the dispersion curves of the phase velocities and electromechanical coupling coefficients for SAW and Lamb waves are obtained. The excitation of Lamb waves up to a frequency of 7.3 GHz was observed experimentally. The resonance curves for Lamb waves have a higher quality factor  $Q$  compared to surface acoustic waves propagating on the same substrates. At a frequency of about 7 GHz, the loaded  $Q$ -factor reaches 3400, while the quality parameter  $Q \times f = 2.4 \times 10^{13}$  Hz. An unusual effect of a significant increase in the  $Q$ -factor of Lamb waves with the frequency increasing from 760 at 1.5 GHz to 3400 at 7 GHz is noted.

**Keywords:** surface acoustic wave, bulk acoustic wave, Lamb wave, single-crystal diamond, aluminum nitride, piezoelectric layered structure

**DOI:** 10.1134/S1063771021010024

## INTRODUCTION

Composite SAW devices based on piezoelectric layered structures (PLS) have demonstrated good parameters in the 1–3 GHz range. For example, in [1], SAW propagation in PLS (Al, Sc)N/diamond was investigated, where the diamond substrate was prepared by chemical vapor deposition and the delay line was chosen as a measuring device. It was found that such PLS has a low acoustic attenuation up to 3 GHz. Lamb waves (LW), which can be used in acoustoelectronic devices and sensors, can be considered a promising alternative to SAW. The theory of LW propagation in an infinite isotropic plate with free boundaries was developed by Lamb in 1917 [2]. Viktorov [3] proposed a systematic description of the acoustic properties of LW propagating in isotropic plates and their applications in technology; in [4], the use of LW in the nondestructive testing of plates was demonstrated. In his monograph [5], Brekhovskikh presented the results of a comprehensive study of waveguide propagation of normal waves in a layered media. LW and other waveguide modes in thin piezoelectric plates made of lithium niobate, lithium tantalate, potassium niobate, and silicosillenite were studied in detail in [6–15]. In particular, it was noted that the electromechanical coupling coefficients (EMCC) of LW and

surface-transverse ( $SH_n$ ) waves can be significantly larger than those for Rayleigh waves in the same crystals. The authors of [16] investigated a large number of PLS based on ST-cut quartz plates coated with ZnO and AlN films and variants for exciting  $SH$ -waves and LW using an interdigital transducer (IDT). In [17], the theoretical basis of elastic wave propagation in a PLS was considered and, as an example, results were obtained for a Me/ZnO/Me/diamond waveguide. Recently, LW in thin films have been actively studied for use in frequency control devices and sensors [18]. Thus, study [19] presents an example of AlN/Si microsensors based on LW for pressure and gravimetric measurements. Paper [20] presents the results for a resonator on a thin AlN film, in which LW was excited using an IDT. These resonators were used as sensitive gas pressure sensors. Using the IDT, the authors of [21] investigated a number of Devices Under Test (DUT) based on thin piezoelectric plates: resonators with a Bragg reflector (Solidly Mounted Resonator, SMR) based on  $50^\circ$   $YX$ -cut of LiTaO<sub>3</sub> (1) and  $X$ -cut of LiNbO<sub>3</sub> (2), as well as a membrane-type resonator (3) based on a  $Z$ -cut of LiNbO<sub>3</sub> to excite SAW and LW. It was found that the device of type (1) had a  $Q$ -factor as of 1735 at a resonance frequency of 3440 MHz in the  $SH_0$  mode; type (2),  $Q = 565$  at 4996 MHz in  $S_0$  Lamb

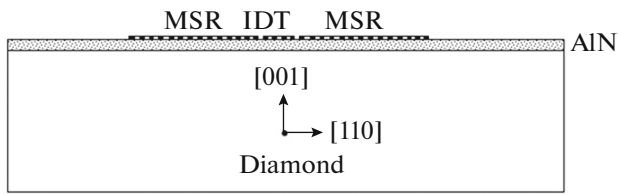


**Fig. 1.** Diagram of SAW resonator with Me-IDT/AlN/diamond structure. SAW propagates along [110] direction in (001) plane of diamond; MSR, multistrip reflector.

mode; and type (3),  $Q = 419$  at 5444 MHz in  $A_1$  Lamb mode. According to the authors of [21], devices of types (1) and (2) demonstrated the best performance in the 3–5 GHz range.

The selection of a suitable substrate material for composite microwave acoustoelectronic devices is critical. Recently, it was shown [22, 23] that the use of single-crystal diamond as a PLS substrate makes it possible to significantly increase the operating frequency of a High overtone Bulk Acoustic Resonator (HBAR) based on bulk acoustic waves (BAW). In particular, BAW excitation in the PLS Al/(001)AlN/Mo/(001) diamond and Al/(Al, Sc) N/Mo/(001) diamond was obtained at a frequency of up to 20 GHz with a loaded  $Q$ -factor of  $\sim 13000$ . Thus, a diamond single crystal should be of great interest as a promising substrate material for studying the SAW and LW.

The aim of this work is to consider the features of SAW and LW excitation and propagation in an Me-IDT/AlN/(100) diamond PLS, including the dispersion characteristics of their parameters in a broad microwave band.

**SAW AND LW EXPERIMENTAL STUDY AT SHF IN PLS Me-IDT/AlN/(100) DIAMOND**

SAW and LW can excited and detected in different ways, including an IDT applied to the surface of the piezoelectric medium. Currently, the technology for IDT manufacturing is well developed, which simplifies the study and application of LW in acoustoelec-

tronic devices and nondestructive testing. Practical application of Rayleigh SAW ( $R$ ) is usually limited to 2–3 GHz due to interaction with air and a significant increase in attenuation. In this sense, LWs propagating predominantly in the bulk of the substrate have a lower attenuation at higher frequencies. Compared to  $SH_n$ - and  $R$ -waves, LW can also have higher phase velocities.

As DUTs, we used single-port SAW resonators, which included an exciting IDT and two multistrip reflectors (MSR) (Fig. 1). Table 1 lists the main parameters of DUTs based on Me-IDT/AlN/(100) diamond PLS for studying SAW and LW propagation. For example, in DUT no. 1, we used unapodized equidistant IDT with an aperture of 350  $\mu\text{m}$  and a period  $d = 18, 20, \text{ and } 22 \mu\text{m}$  for three independent SAW resonators. There were 100 pins in the reflective array; the IDT had 50 pairs of pins. The distance between the IDT and MSR pins was equal to the gap between pins. The IDT synchronization frequency can be calculated using the well-known formula

$$f_0 = V/d, \tag{1}$$

where  $V$  is the phase velocity of Rayleigh waves or LW, and  $d = \lambda$  ( $\lambda$  is the Rayleigh or LW wavelength).

The Me = Pt, Al were chosen as the materials for the IDT electrodes. High-quality synthetic type-IIa single-crystal diamond with a low nitrogen content ( $\sim 60$  ppb), used as the substrate, was grown at the Technological Institute for Superhard and New Carbon Materials by the temperature gradient method under high pressure (5 GPa) and temperature ( $\sim 1750$  K) [24]. The roughness  $R_q$  of the diamond substrates, measured with an atomic force microscope (AFM), was within 0.2–2 nm on an area of  $10 \times 10 \mu\text{m}$ . All metal and piezoelectric AlN layers were deposited with AJA Orion 8 magnetron sputtering equipment. The crystal structure and texture quality of the AlN film were monitored with Panalytical Empyrean X-ray diffraction analysis equipment. Diffraction reflections (00·2) were mainly observed, which indicates a good orientation of aluminum nitride crystallites in the film. The FWHM of the rocking curve (00·2) was of

**Table 1.** Parameters of experimental samples

DUT no.	$d, \mu\text{m}$	Direction of wave propagation	IDT thickness, nm	AlN film orientation/thickness, nm	Orientation/thickness of diamond substrate, $\mu\text{m}$
1	18	[110]	Pt/156	(001)/5530	(001)/180
	20				
	22				
2	20	[110]	Al/135	(001)/4350	(001)/458

about  $0.2^\circ$ . The roughness of the AlN film was less than 3 nm on an area of  $10 \times 10 \mu\text{m}$ .

The frequency response of the DUTs was measured in the microwave range from 0.1 to 8 GHz using an E5071C vector network analyzer and an M 150 probe station. The electrical  $Q$ -factor of the resonance curves of SAW resonator was calculated with the E5071C software and standard calculation methods. The experimental frequency measurement accuracy with this analyzer was of  $\pm 0.1$  kHz or better with an increasing the number of points. The SAW resonator measurements for this study were quite accurate,  $\pm 10$  Hz. It should also be borne in mind that the accuracy in determining the IDT period was of  $\pm(0.1-0.2)$   $\mu\text{m}$ . Thus, the calculated value of the phase velocity error was practically limited by the value  $\pm 1$  m/s. The method for determining the  $Q$ -factor at a level of  $-3$  dB relative to the maximum impedance modulus was used as the main one. The impedance value  $Z_{11e}$  was cleaned with respect to the background. The detailed method for measuring and calculating  $Z_{11e}$  was described earlier [25]. Additional methods based on other resonator frequency response were also used. For example, when choosing the measured time delay parameter,  $\tau_d$ , the  $Q$ -factor was calculated from the ratio  $Q = \pi f_a \tau_d$ , where  $f_a$  is the antiresonance frequency. As a rule, the relative discrepancy between the  $Q$  values calculated by different methods did not exceed 10%.

When measuring the amplitude-frequency response, a sweep from 1001 to 1601 points was used. The analyzer screen simultaneously displayed the following data: the complex characteristics of the reflectance coefficient  $S_{11}$ , total  $Z_{11}$ , and cleaned  $Z_{11e}$  impedances; time delay  $\tau_d$ ; and the Smith diagram.

Let us discuss the experimentally detected waves identified as  $R_n$ - and  $SH_n$ -modes for comparison with Lamb waves. It is important that the simultaneous observation of all SAW and LW was possible using the same SAW resonator. In a detailed study of the frequency dependence of the real part of impedance  $\text{Re}Z_{11e}$  obtained for DUTs nos. 1 and 2, SAW modes were detected in the range up to 700 MHz (Fig. 2). In DUT no. 1, three Rayleigh-type modes as  $R_0$ ,  $R_1$  (Sezawa mode), and  $R_2$  as well as two  $SH$ -type modes ( $SH_0$  and  $SH_1$ ) were observed on three independent SAW resonators with different IDT periods. The specific results are shown in Table 2. Please note that the  $R_n$ -type mode demonstrated a higher loaded  $Q$ -factor compared to the  $SH_n$  modes. The mode selection procedure is discussed below.

Above  $\sim 750$  MHz and up to  $\sim 7.3$  GHz, DUTs nos. 1 and 2 showed a large number of nearly equidistant  $\text{Re}Z_{11e}$  maxima associated with resonance excitation of

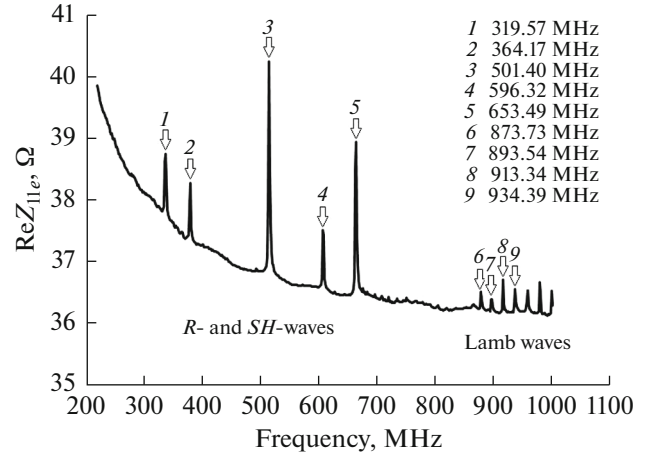


**Fig. 2.** Frequency dependence of real part of impedance  $\text{Re}Z_{11e}$  obtained on DUT no. 1 (SAW resonator with period  $d = 18 \mu\text{m}$ ) in 200–1000 MHz range.

LW of different orders. With increasing frequency, the frequency interval between the  $\text{Re}Z_{11e}$  maxima (Space between Parallel Resonances, SPRF) asymptotically approached the SPRF of an HBAR. As an example, Fig. 3 shows the frequency response of DUTs no. 2 near frequencies of 2.3; 3.5; 5.0 and 7.3 GHz. In addition to strong LW peaks, weaker signals were also observed, which may be related to as yet unidentified modes.

Note that the LW resonance curves showed a significantly higher loaded  $Q$ -factor than that for SAW modes propagating on the same substrate. For DUT no. 2, the  $Q$ -factor was  $Q = 760$  at 1.5 GHz, 1400 at 4 GHz, 2800 at 6.1 GHz, and 3400 at  $\sim 7$  GHz. In the latter case, the quality parameter was  $Q \times f = 2.4 \times 10^{13}$  Hz. As a result, the unusual effect of a significantly increased  $Q$ -factor of the LW peaks with an increasing frequency was established, which is of great practical importance.

#### IDENTIFICATION OF TYPES AND DISPERSION DEPENDENCES OF PARAMETERS OF ELASTIC WAVE PROPAGATION IN A PIEZOELECTRIC LAYERED STRUCTURE

The propagation of various types of small-amplitude acoustic waves in a crystal can be described by wave equations, electrostatic equations, and equations of state of a homogeneous piezoelectric medium, taken in the form [26]

$$\begin{aligned} \rho_0 \ddot{U}_i &= \tau_{ij,j}, \quad D_{k,k} = 0, \\ \tau_{ij} &= C_{ijkl}^E \eta_{kl} - e_{nij} E_n, \quad D_m = \varepsilon_{mn}^1 E_n + e_{mij} \eta_{ij}, \end{aligned} \quad (2)$$

**Table 2.** Results on SAW propagation obtained on DUT no. 1

	Mode	Wavelength, $\mu\text{m}$	Antiresonance frequency $f_0$ , MHz	Loaded $Q$ -factor	Phase velocity, m/s
1	$SH_0$	18	319.57	250	5753
		20	301.27	—	6026
		22	287.55	—	6325
2	$R_0$	18	364.17	350	6552
		20	347.01	—	6940
		22	332.15	—	7304
3	$SH_1$	18	501.40	260	9018
		20	463.66	—	9274
		22	432.78	—	9522
4	$R_1$	18	596.32	300	10728
		20	562.01	—	11240
		22	525.41	—	11559
5	$R_2$	18	653.49	270	11772
		20	606.61	—	12132
		22	564.29	—	12408

where  $\rho_0$  is the crystal density;  $U_i$  is dynamic elastic displacement vector;  $\tau_{ij}$  is the thermodynamic stress tensor;  $D_m$  is the electric induction vector;  $\eta_{ij}$  is the strain tensor;  $C_{ijkl}^E$ ,  $e_{mij}$  and  $\epsilon_{mn}^n$  are the elastic, piezoelectric and clamped dielectric constants, respectively. The comma after a lowercase subscript denotes the spatial derivative, and the coordinate Latin subscripts range from 1 to 3. Hereinafter, the rule of summation over repeating indices will be used.

Let the  $Y$  axis of the working coordinate system be directed along the outer normal to the layer surface and the  $X$  axis coincides with the direction of wave propagation. Elastic wave propagation in a PLS must satisfy the specified boundary conditions. In particular, for the Me/piezoelectric film/substrate structure, the following should be required:

(1) equality to zero of the normal stress tensor components at the Me/vacuum and substrate/vacuum interfaces;

(2) continuity of the normal components of the stress tensor and displacement vectors at the Me/piezoelectric film and piezoelectric film/substrate interfaces;

(3) equality to zero of the electric potential associated with the acoustic wave at the Me/piezoelectric film interface.

As a result, for this problem, we can write the following relations:

$$\begin{aligned}
 \tau_{2j}^{(1)}|_{Y=h_1} &= 0, & \tau_{2j}^{(1)} &= \tau_{2j}^{(2)}|_{Y=h_2}, \\
 \varphi^{(2)} &= 0|_{Y=h_2}, & U^{(1)} &= U^{(2)}|_{Y=h_2}, \\
 \tau_{2j}^{(3)} &= \tau_{2j}^{(2)}|_{Y=0}, & U^{(3)} &= U^{(2)}|_{Y=0}, \\
 \tau_{2j}^{(3)} &= 0|_{Y=-h}.
 \end{aligned} \tag{3}$$

The numbering in superscripts of (1), (2), and (3) determines such structural components as the metal layer, piezoelectric film, and substrate with thicknesses  $h_1$ ,  $h_2$  and  $h$ , respectively. The necessary solutions determining all the parameters of SAW and LW propagation in the Me/piezoelectric film/substrate PLS should be obtained from the equality to zero of the determinant of boundary condition matrix (3), the size of which for a three-layer structure was  $22 \times 22$ . The further course of the solutions does not fundamentally differ from the problem for a four-layer Me1/piezoelectric film/Me1/substrate PLS, which was considered in detail in [25]. For 1D modeling and numerical analysis of the Me/piezoelectric film/substrate PLS, we used our proprietary software.

The procedure for identifying the types of waves was carried out by analyzing the projections of elastic displacements that exactly correspond to each mode.

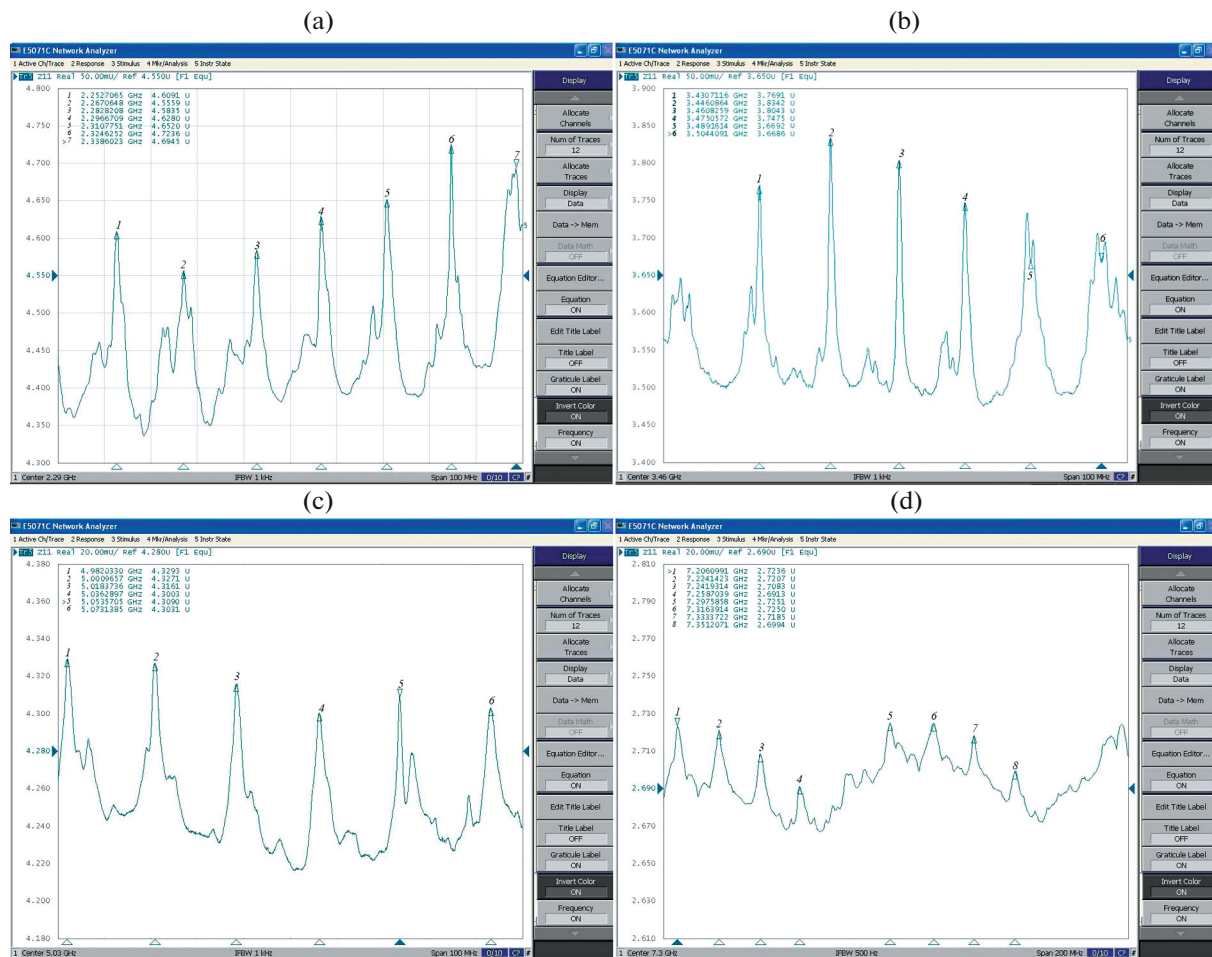


**Fig. 3.** Examples of frequency dependence of real part of impedance  $ReZ_{11e}$  obtained on DUT no. 2 (SAW resonator with period  $d = 20 \mu\text{m}$ ) near frequencies (a) 2.3, (b) 3.5, (c) 5.0, (d) 7.3 GHz.

In a given case, all modes were pure, i.e., displacement vectors with components  $(U_1, U_2, 0)$  and  $(0, 0, U_3)$  were associated with Rayleigh and  $SH$ -type modes, respectively. Note that the condition for the existence of these modes presupposes exponential decay of the partial components as they travel deeper into the diamond substrate. Conversely, the fields of Lamb mode displacements take up the entire bulk of the substrate.

Figure 4 shows, together with experimental data, the results of calculating the dispersion dependences of phase velocities and EMCC for surface-type waves propagating in the  $[110]$  direction of diamond in the Pt/AlN/(001) diamond PLS in the 0–1000 MHz frequency band. The thicknesses of the PLS layers were chosen equal to the corresponding values in DUT no. 1. The parameters of the material properties as the densities and elastic constants of films and single-crystal diamond were taken from [27–29]. Table 2 presents the experimental data on the resonance frequencies and  $Q$ -factor of surface-type modes, as well as identification of their type (see also Fig. 2). The EMCC

(Fig. 4b) were obtained with the well-known formula  $K^2 = 2\Delta V/V$ , where  $\Delta V$  is the change in the SAW phase velocity when an infinitely thin conducting layer is applied to the free surface of piezoelectric medium. It should be noted that the calculated and experimental data are in good agreement.

Naturally, the phase velocity of the fundamental mode  $R_0$  in a PLS has a smaller value than in the case of a nondispersive  $R$ -mode propagating along the  $[110]$  direction along the free (001) surface of diamond, and it tends toward the phase velocity of the  $R$ -mode at zero frequency. Note that such parameters for the Sezawa mode  $R_1$  as the EMCC (Fig. 4b) and phase velocity (Fig. 4a) have larger values than similar ones for the  $R_0$  mode. Therefore, Sezawa mode is preferable for practical application. Rayleigh-type modes also demonstrate higher  $Q$ -factors compared to  $SH$ -modes. Despite the predicted low electromechanical coupling (Fig. 4b),  $SH_0$ - and  $SH_1$ -waves were reliably observed in the experiment (see Fig. 2). As we

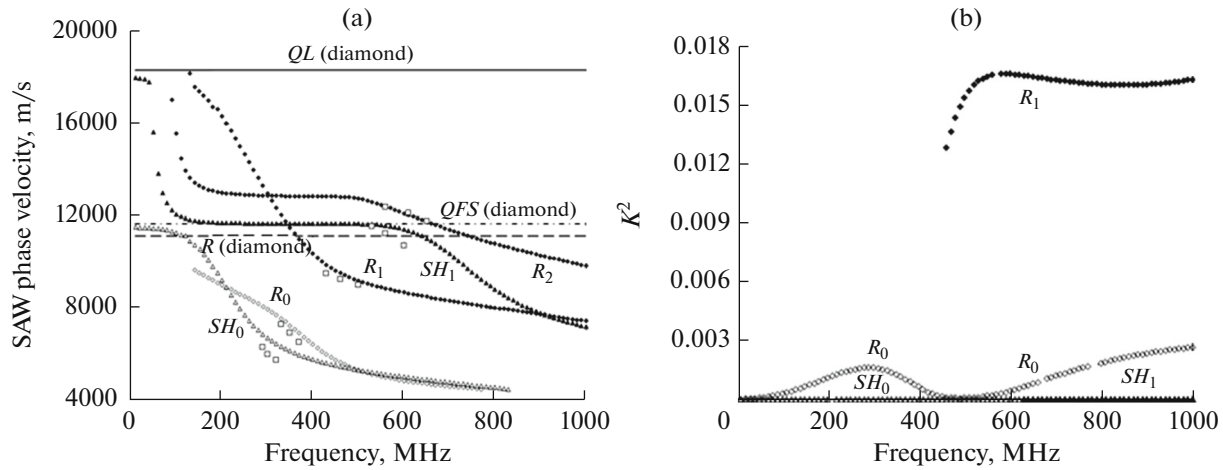


**Fig. 4.** Calculated dispersion curves (a) of phase velocities and (b) EMCC of SAW in Pt/AlN/(001) diamond PLS (SAW propagation is along [110] direction of diamond). Squares, experimental data for sample no. 1. *QL*, *QFS*, and *R* refer to BAW phase velocity curves of quasilongitudinal and quasishear fast type and to Rayleigh SAW in diamond single crystal, respectively.

showed earlier [30], the maximum EMCC for *SH*-modes can be obtained for the Me/(100) AlN/diamond PLS when surface waves propagate along the [010] direction in the (100) plane of aluminum nitride. Therefore, excitement of *SH*-waves in the case of the Me/(001) AlN/(001) diamond configuration can be explained by the imperfection of the texture of aluminum nitride film, due to which the axes of a certain number of crystallites are deflected from the normal to the substrate plane.

LW are attributed to one of the types of normal waves in acoustic waveguides, namely, in a plate with free boundaries [5]. Therefore, first, the existence of LW mode branches of different orders should be limited from below by certain cutoff frequencies and, second, there should be a frequency dependence of phase velocities and other propagation parameters. A distinction should be made between symmetrical  $S_n$  and antisymmetric  $A_n$  Lamb waves, where  $n = 0, 1, 2, 3, \dots$  is the number of dispersion branch. If we assume that LW propagation occurs along the horizontal axis  $X$ , then the particle displacement structure will have horizontal  $U_x$  and vertical  $U_y$  partial components, while the phase shift between them should be  $90^\circ$ ; i.e., oscillating particles move over an ellipse, which in the case of pure modes lies in the sagittal plane  $XY$ . The generation point of  $S_n$  or  $A_n$  modes for  $n > 1$  at the cutoff frequency is determined from the condition that the LW phase velocity turns to infinity. This corresponds to a standing wave along the vertical  $Y$  axis of the plate. Earlier, we pointed out [30] that it is necessary to distinguish modes such as  $S_{n,L}$  or  $S_{n,T}$ , and  $A_{n,L}$  or  $A_{n,T}$ , using the following definition: which of the two BAW modes—longitudinal  $L$  or shear  $T$ , propagating in the vertical  $Y$  direction—is transformed to Lamb-type

wave above the cutoff frequency unique for this mode. A detailed theory of LW propagation in a PLS was published in a chapter of monograph [30].

The frequency range of 1400–1550 MHz was selected as an example for a more detailed analysis. The dispersion curves of LW phase velocity, calculated for the Al/AlN/diamond PLS, are shown in Fig. 5 together with experimental data. The dimensions of this PLS were chosen close to those for DUT no. 2. It is possible to speak about satisfactory agreement between the calculated and experimental results. However, analyzing Fig. 5b, we can see a double structure of closely spaced dispersion curves. This is also confirmed by the experimental data in Fig. 5a. Explanation of this feature of the fine structure of observed peaks requires further experimental and theoretical studies, since analysis of high-order microwave Lamb modes is rather complicated from the aspect of their identification.

Let us turn to the problem of unusual increase in the  $Q$ -factor of LW peaks with frequency increasing. Preliminary estimates show that there is a change in the LW structure in the form of a decrease in the horizontal and increase in the vertical partial component of the wave at higher frequencies. The horizontal partial component can be associated with one of the partial SAW components. As is known, the BAW attenuation is far less than that of SAW. Thus, high-order LW will with frequency increasing tend toward the BAW in diamond, and it can be assumed that LW energy losses should decrease and the  $Q$ -factor increase.

Two-dimensional modeling of LW excitation and propagation processes with the example of the Al-IDT/AlN/(100) diamond PLS was performed using COMSOL Multiphysics software in the Plane Strain

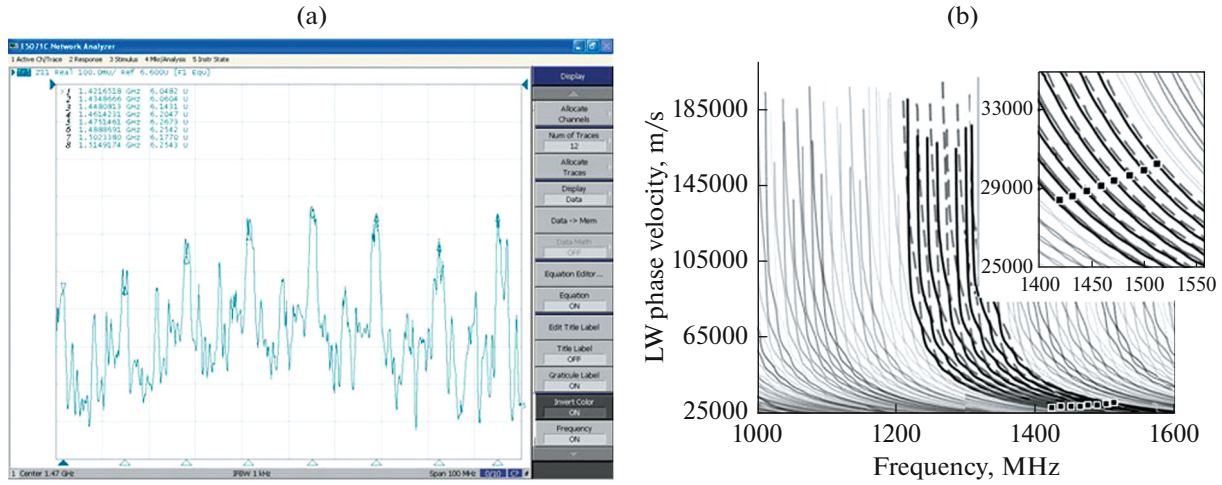


**Fig. 5.** (a) Frequency dependence of real part of impedance  $Re$  of  $Z_{11e}$  obtained on experimental sample no. 2 and (b) calculated dispersion curves of LW phase velocities in Al/AlN/(001) diamond PLS in 1400–1550 MHz frequency range. Squares, experimental data for DUT no. 2.

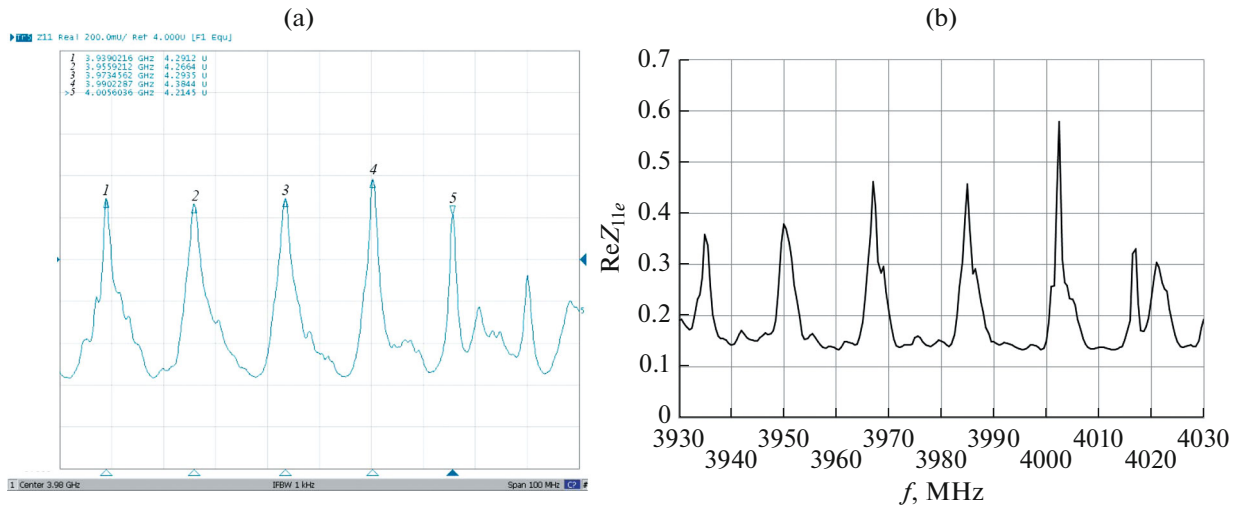


**Fig. 6.** Examples of (a) experimental and (b) calculated frequency dependence of real part of impedance  $Re Z_{11e}$  obtained on DUT no. 2 (SAW resonator with period  $d = 20 \mu\text{m}$ ) near 4 GHz.

approximation. For FEM modeling, a Free Triangular mesh was used, the maximum cell size of which did not exceed  $1/20$  of the sound wavelength in the material under study. We investigated a PLS model with non-apodized IDTs. A microwave signal with a voltage of 1 V was applied to the active IDT electrodes, and the Floating Potential condition was imposed on the reflecting MSR electrodes. The Perfectly Matched Layer (PML) boundary condition was used to prevent acoustic wave reflection from the side walls of sample.

Figure 6 shows the experimental and calculated frequency dependences of the real part of the impedance  $ReZ_{11e}$  obtained near 4 GHz on DUT no. 2 as

SAW resonator with a period  $d = 20 \mu\text{m}$ . The calculation results agree well with the experimental data.

Figure 7 shows the calculation of distribution of the  $Y$ -component of the thickness displacement of DUT no. 2 at 3.968 GHz (one of the resonance peaks shown in Fig. 6). It can be seen that the field of elastic displacements for this mode takes up the entire bulk of the sample. Since the displacements on the upper and lower surfaces of the sample are in phase, it should be concluded that the antisymmetric LW mode occurs in this case. The frequency interval between the  $ReZ_{11e}$  maxima was  $\sim 17$  MHz, while the corresponding value for the HBAR sample achieved on the

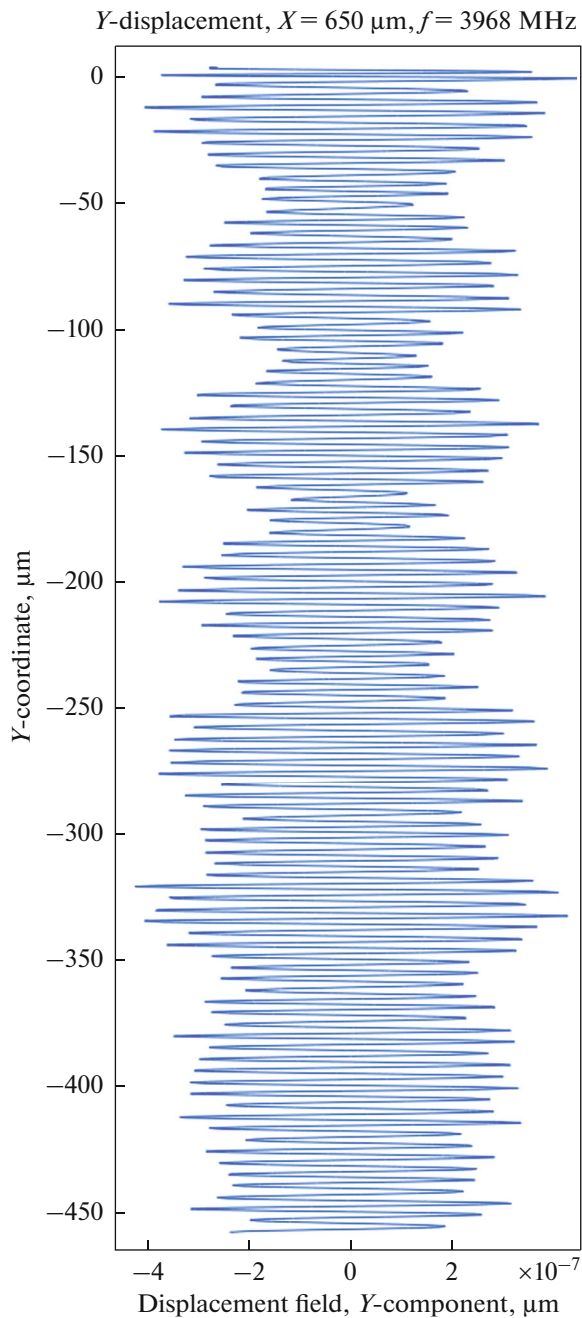


**Fig. 7.** Distribution of  $Y$ -component of thickness displacement of DUT no. 2 (SAW resonator with period  $d = 20 \mu\text{m}$ ) at 3.968 GHz.

Al/AlN/Mo/(100) diamond PLS with the same thicknesses of the substrate and AlN film is  $\sim 19$  MHz.

## CONCLUSIONS

We have studied in detail the propagation of dispersive surface acoustic waves of Rayleigh, Sezawa, and  $SH$ -mode types in the Me-IDT/AlN/(100) diamond (Me = Pt, Al) PLS with a frequency of up to 1000 MHz.

The dispersion curves of the SAW phase velocities and EMCC were obtained and their types identified. For practical application, Sezawa mode  $R_1$  is more preferable, since it has a higher phase velocity and a relatively large EMCC. Rayleigh-type modes show a higher  $Q$ -factor compared to  $SH$ -modes.

LW excitation at microwave frequencies in the Me-IDT/AlN/(100) diamond PLS, configured as a SAW resonator, was achieved in the 750–7300 MHz range. A significantly higher  $Q$ -factor of the LW resonance curves is demonstrated than for SAW propagating on the same substrate. Thus, at a frequency of  $\sim 7$  GHz, the loaded  $Q$ -factor had a value of  $\sim 3400$ , and the quality parameter is equal to  $Q \times f = 2.4 \times 10^{13}$  Hz. These parameters are almost ten times higher than similar data recently obtained for the SMR and membrane resonators based on thin lithium niobate plates in which LW are used and the operating frequencies are limited to 5 GHz [21]. Note also that the LW resonances in the studied samples were observed at higher frequencies up to 7.3 GHz.

Based on the experimental results of this study, the authors propose a detailed analysis of the structure of microwave LW with tools for visualizing the elastic displacement fields in COMSOL Multiphysics, which will be carried out in their next paper.

The results can be useful in developing composite microwave acoustoelectronic devices and sensors.

## FUNDING

The study was financially supported by a grant from the Russian Science Foundation (project no. 16-12-10293-P). Special thanks to S.A. Terentyev and M.S. Kuznetsov (Technological Institute for Superhard and New Carbon Materials) for the preparation of diamond single crystals and substrates.

## REFERENCES

1. K. Hashimoto, T. Fujii, S. Sato, T. Omori, Ch. Ahn, A. Teshigahara, K. Kano, H. Umezawa, and S. Shikata, in *Proc. 2012 IEEE Int. Ultrasonics Symp.* (Dresden, Oct. 7–10, 2012), p. 1926.
2. H. Lamb, *Proc. R. Soc. A* **93**, 114 (1917).
3. I. A. Viktorov, *Physical Foundations of Relay and Lamb Ultrasonic Waves Application in Engineering* (Nauka, Moscow, 1966) [in Russian].
4. T. Ghosh, T. Kundu, and P. Kapur, *Ultrasonics* **36**, 791 (1998).
5. A. M. Brekhovskikh, *Waves in Layered Mediums* (USSR Acad. Sci., Moscow, 1957) [in Russian].
6. Y. Jin and S. G. Joshi, *IEEE Trans. Ultrason., Ferroelectr. Freq. Control* **41**, 279 (1994).
7. Y. Jin and S. G. Joshi, *IEEE Trans. Ultrason., Ferroelectr. Freq. Control* **43**, 491 (1996).



8. I. A. Borodina, S. G. Joshi, B. D. Zaitsev, and I. E. Kuznetsova, *Acoust. Phys.* **46** (1), 33 (2000).
9. S. G. Joshi, B. D. Zaitsev, and I. E. Kuznetsova, *Acoust. Phys.* **47** (3), 282 (2001).
10. I. E. Kuznetsova, B. D. Zaitsev, S. G. Joshi, and I. A. Borodina, *IEEE Trans. Ultrason., Ferroelectr. Freq. Control* **48**, 322 (2001).
11. V. Klymko, A. Nadtochiy, and I. Ostrovskii, *IEEE Trans. Ultrason., Ferroelectr. Freq. Control* **55** (12), 2726 (2008).
12. I. E. Kuznetsova, B. D. Zaitsev, I. A. Borodina, A. A. Teplyh, V. V. Shurygin, and S. G. Joshi, *Ultrasonics* **42**, 179 (2004).
13. B. D. Zaitsev, I. E. Kuznetsova, I. A. Borodina, and S. G. Joshi, *Ultrasonics* **39**, 51 (2001).
14. V. I. Anisimkin, *Acoust. Phys.* **62** (2), 165 (2016).
15. V. I. Anisimkin, E. Verona, A. S. Kuznetsova, and V. A. Osipenko, *Acoust. Phys.* **65** (2), 171 (2019).
16. V. I. Anisimkin and N. V. Voronova, *Acoust. Phys.* **66** (1), 1 (2020).
17. S. I. Burkov, O. P. Zolotova, B. P. Sorokin, P. P. Turchin, and V. S. Talismanov, *J. Acoust. Soc. Am.* **143**, 16 (2018).
18. V. Yantchev and I. Katardjiev, *J. Micromech. Microeng.* **23**, 043001 (2013).
19. A. Choujaa, N. Tirole, C. Bonjour, G. Martin, D. Hauden, P. Blind, and C. Pommier, *Sens. Actuators, A* **46**, 179 (1995).
20. E. Anderås, I. Katardjiev, and V. Yantchev, *J. Micromech. Microeng.* **21**, 85010 (2011).
21. T. Kimura, M. Omura, Y. Kishimoto, and K. Hashimoto, *IEEE Trans. Microwave Theory Tech.* **67**, 915 (2019).
22. B. P. Sorokin, G. M. Kvashnin, A. S. Novoselov, V. S. Bormashov, A. V. Golovanov, S. I. Burkov, and V. D. Blank, *Ultrasonics* **78**, 162 (2017).
23. B. P. Sorokin, A. S. Novoselov, G. M. Kvashnin, N. V. Luparev, N. O. Asafiev, A. B. Shipilov, and V. V. Aksenenkov, *Acoust. Phys.* **65** (3), 263 (2019).
24. Yu. Shvyd'ko, S. Stoupin, V. Blank, and S. Terentyev, *Nat. Photonics* **5**, 539 (2011).
25. B. P. Sorokin, G. M. Kvashnin, A. S. Novoselov, S. I. Burkov, A. B. Shipilov, N. V. Luparev, V. V. Aksenenkov, and V. D. Blank, *Piezoelectricity-Organic and Inorganic Materials and Applications*, Ed. by S. G. Vasiliadis and D. Matsouka (IntechOpen, 2018), p. 15.
26. K. S. Aleksandrov, B. P. Sorokin, and S. I. Burkov, *Efficient Piezoelectric Crystals for Acoustical Electronics, Piezoengineering and Sensors* (Siberian Branch RAS, Novosibirsk, 2007), **Vol. 1** [in Russian].
27. A. V. Sotnikov, H. Schmidt, M. Weihnacht, T. Yu. Chemekova, and Yu. N. Makarov, *IEEE Trans. Ultrason., Ferroelectr. Freq. Control* **57**, 808 (2010).
28. B. P. Sorokin, G. M. Kvashnin, A. V. Telichko, G. I. Gordeev, S. I. Burkov, and V. D. Blank, *Acoust. Phys.* **61** (4), 422 (2015).
29. J. A. Rayne and C. K. Jones, *Phys. Lett.* **18**, 91 (1965).
30. B. P. Sorokin, G. M. Kvashnin, A. V. Telichko, S. I. Burkov, and V. D. Blank, in *Piezoelectric Materials*, Ed. by T. Ogawa. Rijeka (Intech, 2016), p. 161.